ISSN 1063-7710, Acoustical Physics, 2019, Vol. 65, No. 3, pp. 235–245. © Pleiades Publishing, Ltd., 2019.

CLASSICAL PROBLEMS OF LINEAR ACOUSTICS AND WAVE THEORY

Acoustic Field Excited by Single Force with Arbitrary Direction in Semi-Infinite Elastic Space[1]

Yuxiang Dai[a, b], Shouguo Yan[a, *], and Bixing Zhang[a]

[a] *Key Laboratory of Acoustics, Institute of Acoustics, Chinese Academy of Sciences, Beijing, 100190 China*

[b] *University of Chinese Academy of Sciences, Beijing, 100190 China*

**e-mail: yanshouguo@mail.ioa.ac.cn*

Received October 24, 2018; revised December 3, 2018; accepted December 26, 2018

Abstract—In this paper, the acoustic field excited by a single force with arbitrary direction in a semi-infinite elastic space is studied and its mathematical expressions are obtained. It shows that there are many complex behaviors when the elastic wave reaches the free boundary. The numerical simulation shows that there are several kinds of waves in the semi-infinite elastic space: direct P wave, direct SV wave, SP wave propagating along the free surface which can generate Head wave and Rayleigh wave. The forming mechanism of the SP wave and Rayleigh wave is specially studied. The waveforms at the observation point on the free surface of the semi-infinite space contain only direct P wave and direct SV wave when the SV wave incident angle is within the critical reflection angle. However, if the incident angle from the source to the observation point is exceeding to the critical reflection angle, not only direct P and direct SV wave but also the SP wave and Rayleigh wave are all be generated. It is focused on the relationships of the direction of single force to the excitation intensity of each wave. The relationship of each wave packet to the single force and observation direction is obtained and analyzed.

Keywords: semi-infinite elastic space, single force with arbitrary direction, excitation intensity of each wave, SP wave

DOI: 10.1134/S1063771019030102

1. INTRODUCTION

The acoustic field in semi-infinite elastic space radiated by different kinds of force systems was originally studied in the area of seismic waves. Lamb was the first to study the propagation of a pulse in an elastic half space. In 1904, Lamb treated four basic problems: the surface normal line sources, the point load sources, the buried line sources and point sources of dilatation, which has taken on the name Lamb's problem. More researches on Lamb's problem have been studied [1–5]. And the mathematical expressions of the displacements of the acoustic field due to several types of force systems were investigated and obtained [6–9], including a single force. However, in most of these works, the single force is along or perpendicular the surface direction of the semi-infinite elastic space [5, 10]. The acoustic problems related to this situation have been studied and applied to other field, such as the surface waves [11–15] and wave propagation in media with different boundary conditions [16–21]. Nevertheless, some acoustic problems related to the excitation and propagation characteristic of the waves in semi-infinite media are not sufficiently studied and described. In this paper, the acoustic field excited by a single force with an arbitrary direction in a semi-infinite elastic space is studied. The mathematical expressions of the acoustic field are obtained and acoustic propagation characteristics are analyzed with the *B*, *P*, *C* coordinate system. The relationships of the direction of single force to the excitation intensity of each wave on the free surface is deeply analyzed through the numerical simulation of the response of acoustic field at different positions, and several useful conclusions are obtained. Compared with other studies, for example [5], the mathematical expressions in this paper have very explicit physical meanings and can show us how each wave will propagate when they reach the boundary. Comparing to [5], this paper is focused on the influence of the direction of the force on each wave, especially the SP wave and Rayleigh wave. It is found that only the SP wave reflected by SV wave incident at the critical reflection angle can propagate along the boundary. And on the propagation path in the direction of the single force, only P wave can propagate, which makes it that the SP wave cannot be formed when the direction of single force is equal to the critical reflection angle. It is also found that the inhomogeneous SP wave turns into the Rayleigh wave, in order to satisfy the free boundary conditions. Besides, the relationship of the Rayleigh wave inten-

[1] The article is published in the original.

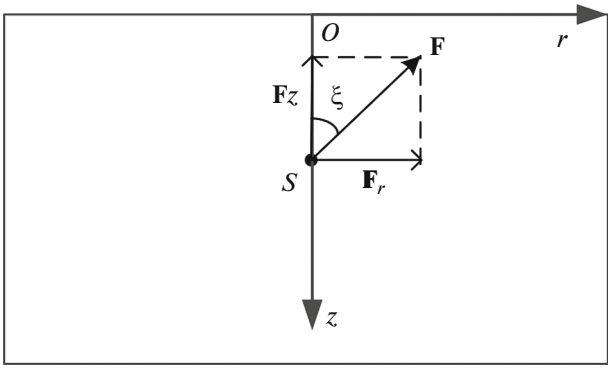

Fig. 1. Model configuration.

sity to relative depth of source and the direction of single force is obtained.

2. PROBLEM STATEMENT

It is convenient to introduce certain fundamental solutions of the motion equations in the cylindrical coordinate system (r, θ, z) in order to solve the three-dimensional problem. The semi-infinite elastic space is distributed in $z \geq 0$. In Fig. 1, only a plane with $\theta = 0$ is given. There is a single force **F** distributed along an arbitrary direction at point S inside the elastic semi-infinite medium. We can adjust the direction of the cylinder coordinate system to make this force located inside the r–z plane of the coordinate system and located on the z-axis. Then the force **F** can be decomposed into a force $\mathbf{F}_z$ along the z-axis and a force $\mathbf{F}_r$ along the r-axis. Thus, the displacements duo to **F** can be the superposition of the displacements due to $\mathbf{F}_z$ and $\mathbf{F}_r$.

2.1. Introduction of B, P, C Coordinate System

Let φ, ψ and χ be the displacement potentials of the P, SV and SH waves in the semi-infinite elastic space. The integral solutions in Bessel–Fourier transformation can be written as [22, 23]

$$\begin{aligned}
\varphi(r,\theta,z,\omega) &= \sum_{n=0}^{\infty}\int_0^{\infty}\varphi_n(k,z,\omega)J_n(kr)\cos(n\theta)\,kdk,\\
\psi(r,\theta,z,\omega) &= \sum_{n=0}^{\infty}\int_0^{\infty}\psi_n(k,z,\omega)J_n(kr)\cos(n\theta)\,kdk, \quad (1)\\
\chi(r,\theta,z,\omega) &= \sum_{n=0}^{\infty}\int_0^{\infty}\chi_n(k,z,\omega)J_n(kr)\sin(n\theta)\,kdk,
\end{aligned}$$

where ω is the angular frequency, k is the horizontal wave number, and the n is dependent on the source.

The B, P, C coordinate system was first introduced by Ben-Menahem [21] in 1968. It is convenient to introduce B, P, C coordinate system for wave propagation in a semi-infinite space. In B, P, C coordinate system the displacements expressed by potentials can be written as

$$\mathbf{u} = \nabla\varphi + \nabla\times(\chi\mathbf{e}_z) + \nabla\times\nabla\times\left(\frac{1}{k}\psi\mathbf{e}_z\right), \quad (2)$$

where the potential ψ has been substituted by $k\psi$ for convenience.

The B, P, C coordinate system is a transformation of the cylindrical coordinate system. Its base vector can be written as

$$\begin{aligned}
\mathbf{B} &= \frac{\partial}{\partial(kr)}\mathbf{e}_r + \frac{\partial}{kr\partial\theta}\mathbf{e}_\theta, \quad \mathbf{P} = \mathbf{e}_z,\\
\mathbf{C} &= \frac{\partial}{kr\partial\theta}\mathbf{e}_r - \frac{\partial}{\partial(kr)}\mathbf{e}_\theta.
\end{aligned} \quad (3)$$

Then, the displacements can be written as

$$\mathbf{u} = u_B\mathbf{B} + u_P\mathbf{P} + u_C\mathbf{C}, \quad (4)$$

with

$$u_B = k\varphi + \frac{\partial\psi}{\partial z}, \quad u_P = \frac{\partial\varphi}{\partial z} + k\psi, \quad u_C = k\chi,$$

and the stress components can be written as

$$\boldsymbol{\tau} = \tau_B\mathbf{B} + \tau_P\mathbf{P} + \tau_C\mathbf{C}, \quad (5)$$

with

$$\tau_B = 2\mu\left(k\frac{\partial\varphi}{\partial z} + \Omega\psi\right), \quad \tau_P = 2\mu\left(\Omega\varphi + k\frac{\partial\psi}{\partial z}\right),$$
$$\tau_C = \mu k\frac{\partial\chi}{\partial z},$$

where: $\Omega = k^2 - \frac{1}{2}k_s^2$.

From Eqs. (4) and (5), it can be found that the SH wave is also decoupled independently in B, P, C coordinate system. Thus, we can just consider the situation of the P–SV wave in B, P, C coordinate system. Then, the displacement vector Eq. (2) become

$$\mathbf{u} = \nabla\varphi + \nabla\times\nabla\times\left(\frac{1}{k}\psi\mathbf{e}_z\right). \quad (6)$$

According to the relationship between B, P, C coordinate system and cylindrical coordinate system, the displacements in cylindrical coordinate system can be written as

$$u_r = \frac{\partial}{\partial r}\left(\varphi + \frac{1}{k}\frac{\partial\psi}{\partial z}\right), \quad u_z = u_P = \frac{\partial\varphi}{\partial z} + k\psi. \quad (7)$$

2.2. The Acoustic Field Response

Considering a source exciting the acoustic field at the point $z = z_s$, the integral solutions of the displace-

ment potentials in Bessel–Fourier transformation with the omitted time factor $\exp(-i\omega t)$ for general P–SV source can be written as

$$\begin{aligned}&\varphi^s(r,\theta,z,\omega)\\&=\sum_{n=0}^{\infty}\int_0^{\infty}A_n^s\exp(i\alpha|z-z_s|)J_n(kr)\cos(n\theta)\,kdk,\\&\psi^s(r,\theta,z,\omega)\\&=\sum_{n=0}^{\infty}\int_0^{\infty}B_n^s\exp(i\beta|z-z_s|)J_n(kr)\cos(n\theta)\,kdk,\end{aligned}\tag{8}$$

where $\alpha=\sqrt{k_P^2-k^2},\beta=\sqrt{k_S^2-k^2}$, k_P and k_S are the wave numbers of the P and SV waves, and the coefficients A_n^s and B_n^s are known for a definite source.

Similarly, the reflection displacement potentials excited by the interface ($z=0$) propagates along the z-axis direction and can be written as

$$\begin{aligned}&\varphi^r(r,\theta,z,\omega)\\&=\sum_{n=0}^{\infty}\int_0^{\infty}C(k,\omega)\exp(i\alpha z)J_n(kr)\cos(n\theta)\,kdk,\\&\psi^r(r,\theta,z,\omega)\\&=\sum_{n=0}^{\infty}\int_0^{\infty}D(k,\omega)\exp(i\beta z)J_n(kr)\cos(n\theta)\,kdk.\end{aligned}\tag{9}$$

Then, the total field in semi-infinite space is

$$\begin{aligned}\varphi&=\varphi^s(r,\theta,z,\omega)+\varphi^r(r,\theta,z,\omega)\\&=\sum_{n=0}^{\infty}\int_0^{\infty}\left[A_n^s\exp(i\alpha|z-z_s|)+C_n\exp(i\alpha z)\right]\\&\quad\times J_n(kr)\cos(n\theta)\,kdk,\\\psi&=\psi^s(r,\theta,z,\omega)+\psi^r(r,\theta,z,\omega)\\&=\sum_{n=0}^{\infty}\int_0^{\infty}\left[B_n^s\exp(i\beta|z-z_s|)+D_n\exp(i\beta z)\right]\\&\quad\times J_n(kr)\cos(n\theta)\,kdk.\end{aligned}\tag{10}$$

At the surface of the medium, the boundary conditions can be written as

$$\tau_B\big|_{z=0}=0,\quad \tau_P\big|_{z=0}=0.\tag{11}$$

By Eqs. (5), (10) and (11), we can get

$$\begin{aligned}&-ki\alpha\left[A_n^s\exp(i\alpha z_s)-C_n\right]\\&+\Omega\left[B_n^s\exp(i\beta z_s)+D_n\right]=0,\\&\Omega\left[A_n^s\exp(i\alpha z_s)+C_n\right]\\&-ki\beta\left[B_n^s\exp(i\beta z_s)-D_n\right]=0.\end{aligned}\tag{12}$$

It is easy to get the solution

$$\begin{aligned}C_n&=\frac{1}{S}\left[TA_n^s\exp(i\alpha z_s)+\frac{2ik\Omega}{\alpha}B_n^s\exp(i\beta z_s)\right],\\D_n&=\frac{1}{S}\left[\frac{2ik\Omega}{\beta}A_n^s\exp(i\alpha z_s)+TB_n^s\exp(i\beta z_s)\right].\end{aligned}\tag{13}$$

where $S=k^2+\dfrac{\Omega^2}{\alpha\beta}$, $T=k^2-\dfrac{\Omega^2}{\alpha\beta}$.

Then, the displacement potentials in a semi-infinite space have been obtained as the following:

$$\begin{aligned}\varphi(r,\theta,z,\omega)&=\sum_{n=0}^{\infty}\int_0^{\infty}\left\{A_n^s\exp(i\alpha|z-z_s|)+\frac{T}{S}A_n^s\exp[i\alpha(z+z_s)]\right.\\&\left.+\frac{k}{\alpha}\frac{2i\Omega}{S}B_n^s\exp(i\beta z_s)\exp(i\alpha z)\right\}J_n(kr)\cos(n\theta)\,kdk,\\\psi(r,\theta,z,\omega)&=\sum_{n=0}^{\infty}\int_0^{\infty}\left\{B_n^s\exp(i\beta|z-z_s|)+\frac{T}{S}B_n^s\exp[i\beta(z+z_s)]\right.\\&\left.+\frac{k}{\beta}\frac{2i\Omega}{S}A_n^s\exp(i\alpha z_s)\exp(i\beta z)\right\}J_n(kr)\cos(n\theta)\,kdk.\end{aligned}\tag{14}$$

Eqs. (14) show that the P (or SV) wave cannot satisfy the free boundary conditions at the surface independently. So, when a P (or SV) wave reaches the boundary of the semi-infinite space, it generates not only the reflected P (or reflected SV) wave, but also the converted SV (or converted P) wave.

2.3. The Acoustic Field Excited by a Single Force with Arbitrary Direction

In this section, the acoustic field for a single force with arbitrary direction is studied and the displacement potentials are obtained. Only the case, when the single force is along the z-axis (vertical single force) or

perpendicular to the z-axis (horizontal single force), is studied in previous references.

When the single force is along the z-axis, the acoustic field is symmetric and independent on the angle θ. The coefficients A_n^s and B_n^s in Eqs. (8) are [22]

$$A_n^s = \frac{F(\omega)}{4\pi\rho\omega^2}\varepsilon\delta_{n0}, \quad B_n^s = i\frac{F(\omega)}{4\pi\rho\omega^2}\frac{k}{\beta}\delta_{n0}. \tag{15}$$

The value of ε is 1 for $z > z_s$ and -1 for $z < z_s$, and $F(\omega)$ is the Fourier transform of the time function of the single force. Then, the displacement potentials in Eqs. (14) become

$$\begin{aligned}\varphi_0(r,\theta,z,\omega) &= \frac{F(\omega)}{4\pi\rho\omega^2}\int_0^\infty\left\{\varepsilon\exp(i\alpha|z-z_s|) + \frac{T}{S}\varepsilon\exp[i\alpha(z+z_s)]\right.\\ &\left. - \frac{2\Omega k^2}{\alpha\beta S}\exp(i\beta z_s)\exp(i\alpha z)\right\}J_0(kr)\,kdk,\\ \psi_0(r,\theta,z,\omega) &= \frac{ikF(\omega)}{4\pi\rho\omega^2\beta}\int_0^\infty\left\{\exp(i\beta|z-z_s|) + \frac{T}{S}\exp[i\beta(z+z_s)]\right.\\ &\left. + \frac{2\Omega}{S}\varepsilon\exp(i\alpha z_s)\exp(i\beta z)\right\}J_0(kr)\,kdk.\end{aligned} \tag{16}$$

When the single force is perpendicular to the z-axis, the coefficients A_n^s and B_n^s in Eqs. (8) are [22]

$$A_n^s = i\frac{F(\omega)}{4\pi\rho\omega^2}\frac{k}{\alpha}\delta_{n1}, \quad B_n^s = \frac{F(\omega)}{4\pi\rho\omega^2}\varepsilon\delta_{n1}. \tag{17}$$

In this case, the displacement potentials in Eqs. (14) become

$$\begin{aligned}\varphi_1(r,\theta,z,\omega) &= \frac{ikF(\omega)}{4\pi\alpha\rho\omega^2}\int_0^\infty\left\{\exp(i\alpha|z-z_s|) + \frac{T}{S}\exp[i\alpha(z+z_s)]\right.\\ &\left. + \frac{2\Omega}{S}\varepsilon\exp(i\beta z_s)\exp(i\alpha z)\right\}J_1(kr)\cos(\theta)\,kdk,\\ \psi_1(r,\theta,z,\omega) &= \frac{F(\omega)}{4\pi\rho\omega^2}\int_0^\infty\left\{\varepsilon\exp(i\beta|z-z_s|) + \frac{T}{S}\varepsilon\exp[i\beta(z+z_s)]\right.\\ &\left. - \frac{2\Omega k^2}{\alpha\beta S}\exp(i\alpha z_s)\exp(i\beta z)\right\}J_1(kr)\cos(\theta)\,kdk.\end{aligned} \tag{18}$$

For a single force with arbitrary direction, as shown in Fig. 1, the single force $F(\omega)$ is decomposed into a vertical single force $F_z(\omega) = F(\omega)\cos\xi$ and a horizontal single force $F_r(\omega) = F(\omega)\sin\xi$. It can be seen that the displacement potentials generated by vertical single force $F_z(\omega)$ are independent on the angle θ and displacement potentials generated by horizontal single force $F_r(\omega)$ have the angle factor cosθ. It is also easy to find by Eqs. (16) and (18) that the displacement potentials for the single force with arbitrary direction can be written as

$$\begin{aligned}\varphi(r,\theta,z,\omega) &= \varphi_0(r,\theta,z,\omega)\cos\xi\\ &+ \varphi_1(r,\theta,z,\omega)\sin\xi,\end{aligned} \tag{19}$$

where $\varphi_0(r,\theta,z,\omega)$ and $\varphi_1(r,\theta,z,\omega)$ are given by Eqs. (16) and (18) respectively. It can be seen by Eq. (19) that the displacement potentials contain the items independent on the angle θ and related cosθ.

The displacement about the single force with arbitrary direction can be obtained by Eqs. (6) and (7). Then, the displacement field in the time domain can be calculated by the Fourier transformation in numerical simulation.

2.4. Numerical Simulation and Propagation Characteristic of Each Wave Packet

There are many complex behaviors when the elastic wave reaches the boundary. In this section, the propagation and characteristics of the elastic wave in semi-infinite space are studied and analyzed through numerical simulation.

Table 1. The parameters for numerical simulation

Density ρ, kg/m^3	P wave velocity c_p, m/s	SV wave velocity c_s, m/s	Rayleigh wave velocity c_r, m/s	Center frequency f_0, kHz	Pulse width t_c, μs
7870	5770	3140	2907	500	5

Table 2. The parameters of a vertical single force for numerical simulation

Point name	Source name	Depth of source z_s, mm	Horizontal position r, mm	Vertical position z, mm
A	S	40	20	0
B	S	40	500	0

A cosine envelope pulse is chosen to be the time function of the single force for numerical simulation, and its expressions in the time domain can be written as

$$f(t) = \frac{1}{2}\left\{1 + \cos\left[\frac{2\pi}{t_c}\left(t - \frac{t_c}{2}\right)\right]\right\} \times \cos\left[2\pi f_0\left(t - \frac{t_c}{2}\right)\right][H(t) - H(t - t_c)],$$

where $f(t)$ is just the Fourier Transformation of $F(\omega)$, t_c is the pulse width in the time domain, f_0 is the center frequency and $H(t)$ is step function.

Here, the parameters of the semi-infinite medium, pulse width and center frequency of the source for numerical simulation are given in Table 1. The time domain waveform $f(t)$ of the single force is given in Fig. 2, in which the amplitude has been normalized.

The time domain waveform of source function $f(t)$ is given in Fig. 2, where all the amplitudes have been normalized.

I. The Simplest Case: a Vertical Single Force ($\xi = 90°$)

For a vertical single force, the acoustic field is symmetrical about the z-axis and independent of θ. The parameters in Eqs. (16) and (18) for numerical simulation are given in Table 2. Here, as shown in Fig. 3, two points A and B on the boundary are chosen as the observation points in order to analyze the response of acoustic field at different positions.

The particle displacements at the points A and B are numerical simulated and shown in Fig. 4. The real and dotted lines are the vertical and horizontal components of the particle displacement respectively.

As shown in Fig. 4a, there are two kinds of wave packets. According to the arrival times of wave, it can be judged that they correspond to the direct P and SV waves respectively. It can be also seen from Fig. 4b that there are four kinds of wave packets. It can be judged that they correspond to the direct P wave, the SP wave, the direct SV wave, and the Rayleigh wave respectively. All the wave packets in Fig. 4 are analyzed and discussed as the following.

A. Analysis of the Packets in Full Waveforms

In order to analyze the cause of formation of the SP wave and Rayleigh wave, it is necessary to consider the reflection of SV wave on the surface. Fig. 5 gives the schematic of the reflection of SV wave on the free surface. According to the boundary conditions, the wave

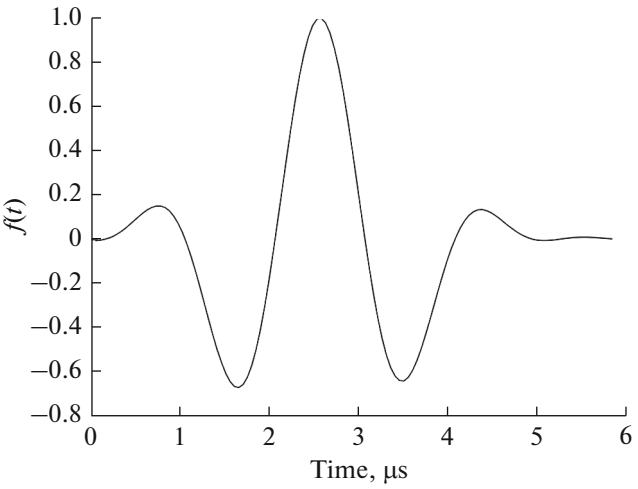

Fig. 2. The time domain waveform of the single force.

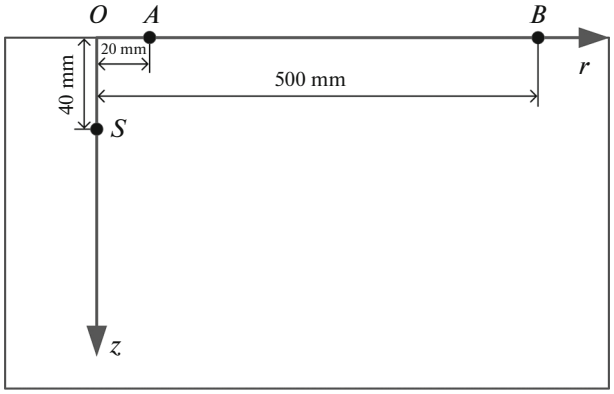

Fig. 3. Sketch of the location of the observation points.

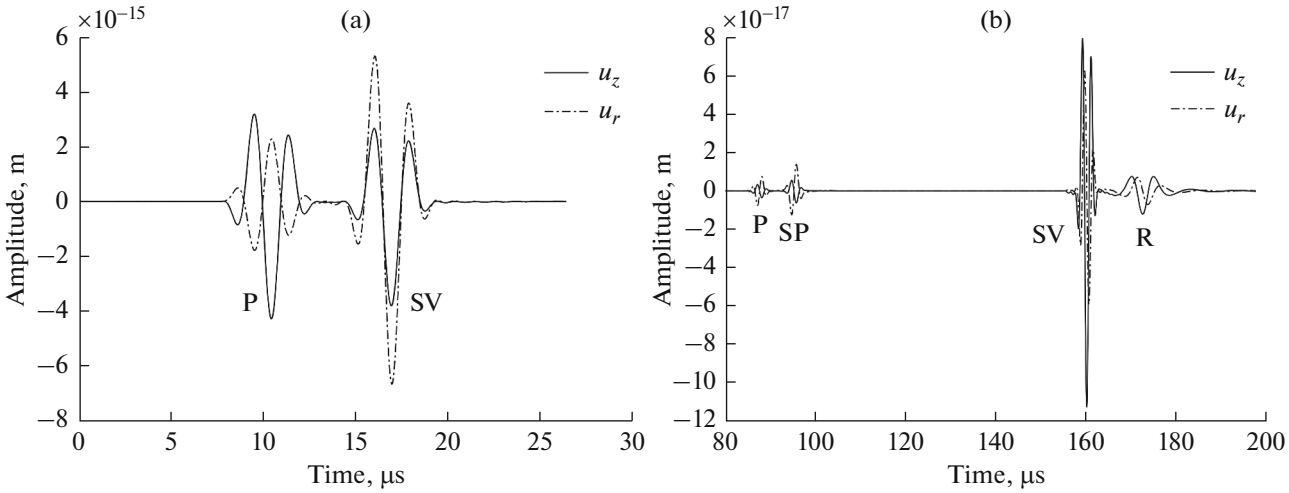

Fig. 4. The particle displacement waveforms: (a) and (b) are for points *A* and *B* respectively.

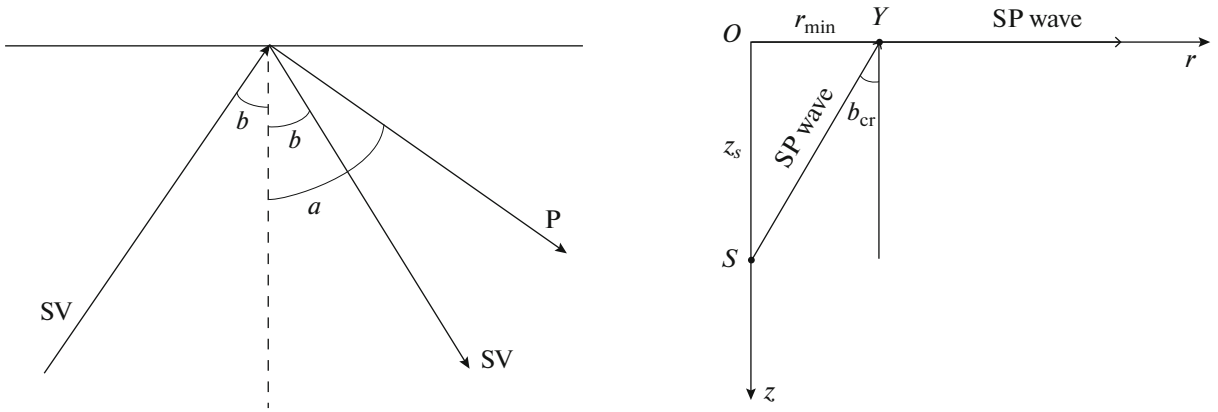

Fig. 5. The schematic of the reflection of SV wave on the boundary.

numbers of the incident SV wave and reflected P wave in the horizontal direction must be equal

$$\frac{\omega}{c_s}\sin b = \frac{\omega}{c_p}\sin a, \tag{20}$$

where b is the incident angle of SV wave, a is the reflection angle of P wave.

With the incident angle of the SV wave increases, the reflection angle of P wave will increase to $\pi/2$ first. So, as shown in Fig. 5b, there is a critical angle b_{cr} for SV wave when it is reflected on the boundary. When the SV wave is incident to the boundary at the critical angle, it will generates a critical homogeneous P wave which propagates along the surface with a velocity of c_p, which is named as the SP wave. In Fig. 5b, the point Y is the critical point where the SP wave can be formed. But this SP wave cannot satisfy the free boundary conditions when propagating independently along the boundary, so it will radiate Head wave [24–27] into the half space as it propagates. The critical angle can be calculated by the following:

$$b_{cr} = \sin^{-1}\left(\frac{c_s}{c_p}\right). \tag{21}$$

If the incident angle exceeds b_{cr}, the reflection angle of SP wave will become a complex number, which makes it that the SP wave becomes a kind of inhomogeneous wave. Similarly, the inhomogeneous SP wave cannot satisfy the free boundary conditions when propagating independently along the boundary. But it cannot radiate Head wave, because in this case the inhomogeneous SP wave is a kind of surface wave, which means that its energy cannot leave the surface. In this case, the inhomogeneous SP wave will turn into Rayleigh wave in order to satisfy the free boundary conditions. So, the inhomogeneous SP wave cannot be observed on the boundary.

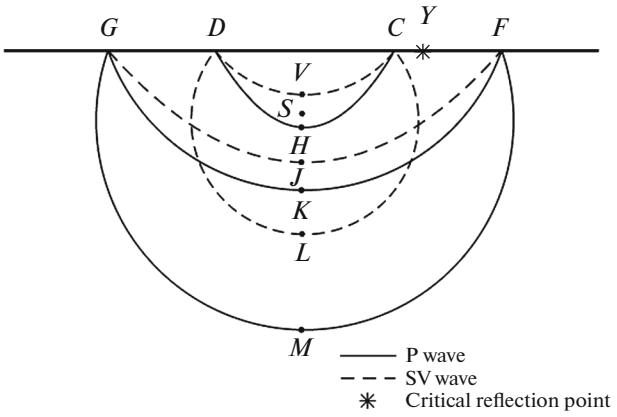

Fig. 6. Distribution of wavefronts of various waves when SV wave is incident within b_{cr}.

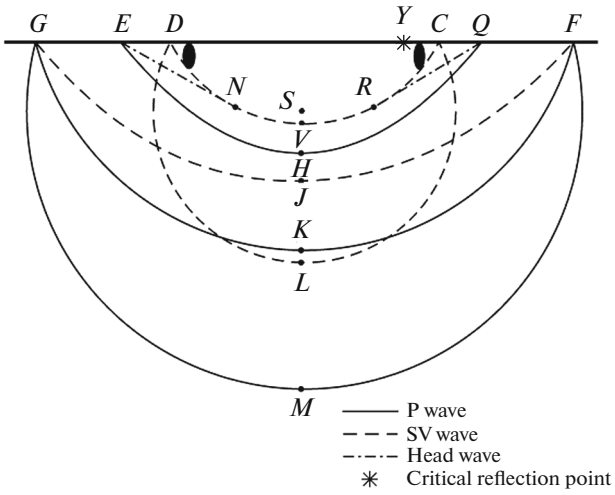

Fig. 7. Distribution of wavefronts of various waves when SV wave is incident exceeding b_{cr}.

So, as shown in Fig. 5b, only the SP wave reflected by SV wave incident at the incident angle b_{cr} can propagate along the boundary, and radiate Head wave.

And there is a minimum horizontal distance from the source to the receiver for the SP wave being formed:

$$r_{min} = \tan b_{cr} z_s. \quad (22)$$

For the medium parameters in this paper, the critical angle b_{cr} is 32.97° and r_{min} is 25.95 mm. So, there is no SP wave at the point *A* with horizontal distance 20 mm. However, at the point *B*, whose horizontal distance is 500 mm, the SP wave can be observed.

Therefore, it can be confirmed that the packets in the full waveforms at the surface should be the direct P wave and the direct SV wave if the horizontal distance from the source to the receiver is less than r_{min} , and be the direct P wave, the SP wave, direct SV wave, and the Rayleigh waves if the horizontal distance from the source to the receiver is greater than r_{min}.

Then, the wavefront distribution in space for each packet is analyzed. It is considered in two cases: the SV wave is incident to the boundary within the critical angle and exceeding the critical angle. The distribution of wavefronts of various wave packets in two cases is plotted in Figs. 6 and 7, respectively.

Figure 6 gives the distribution of all wavefronts at the same time when the SV wave is incident to the surface with incident angle $b < b_{cr}$. As shown in Fig. 6, the direct P wave firstly arrives with wavefront the Arc *GMF*. The P wave reaches the surface and generates the reflected P wave (Arc *GKF*) and the converted SV wave (Arc *GJF*). Then the direct SV wave arrives at the surface with wavefront Arc *DLC*. Similarly, it generates the reflected SV wave (Arc *DVC*) and the converted P wave (Arc *DHC*). This result matches the mathematical expressions perfectly. As shown in Eqs. (14), (16) and (18), each displacement potential includes three parts: the direct wave, the reflected wave, and the converted wave.

Figure 7 depicts the distribution of all wavefronts at the same time in which the SV wave is incident to the surface with incident angle $b > b_{cr}$. In this case, not only the wavefronts with Arc *GMF*, *GKF*, *GJF*, *DLC*, and *DVC* are the same as that in Fig. 6, but also the *SP* wave (points *E*, *Q*) and Rayleigh wave (black area in Fig. 7) should be generated. However, because the propagation velocity of the SP wave is greater than that of the SV wave, the wavefront of reflected P wave is separated from that of the SV wave. In Fig. 7, the wavefront of reflected P wave is *EHQ*.

It had been shown that only the SP wave can be generated and propagated along the surface when the SV wave is incident to the surface with the critical angle b_{cr}. The Head wave (tangent segment *EN* and *QR*) [24–27] could be generated as the SP wave propagated along the surface. When the SV wave is incident to the boundary exceeding the critical angle, the inhomogeneous SP wave is generated but instantaneously form the Rayleigh wave due to the free boundary conditions. So, the inhomogeneous SP wave cannot be observed.

B. The Relationship between Intensity of Rayleigh Wave and the Source Depth

The excitation intensity of the Rayleigh wave in Fig. 4b is relatively weak because the source depth is too deep compared with the wavelength of the Rayleigh wave. If the source depth is decreased, the displacement waveforms at point *B* will be increases significantly. Figure 8 gives a typical example of the Rayleigh wave, in which case the depth of source is 10 mm.

As shown in Fig. 8, the intensity of the Rayleigh wave is significantly improved in this case. Obviously,

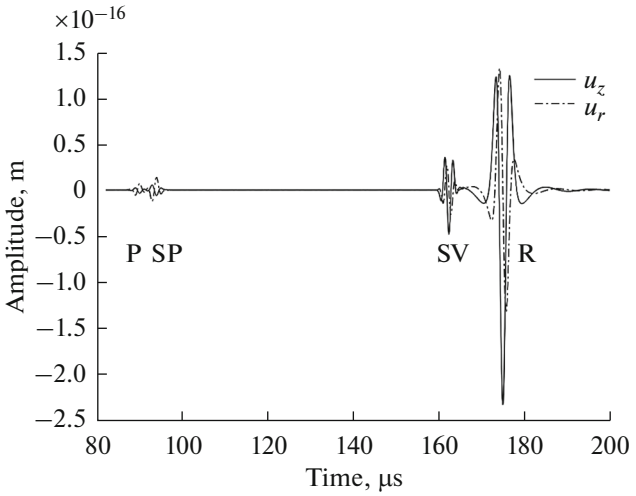

Fig. 8. The displacement waveforms of point *B* with the source depth of 10 mm.

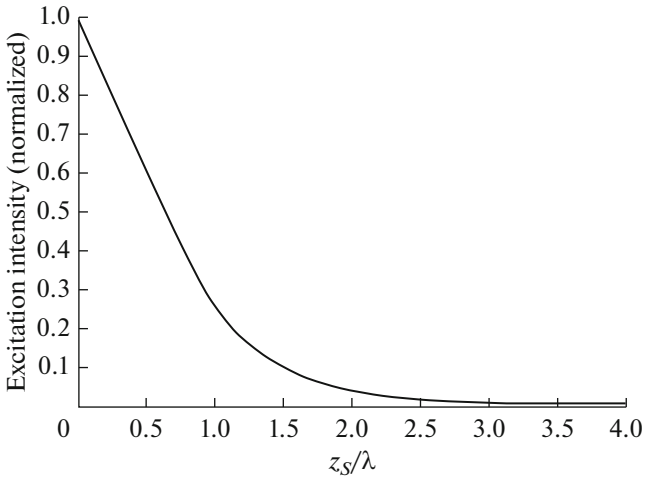

Fig. 9. Relationship of the Rayleigh wave intensity to ratio of source depth to wavelength.

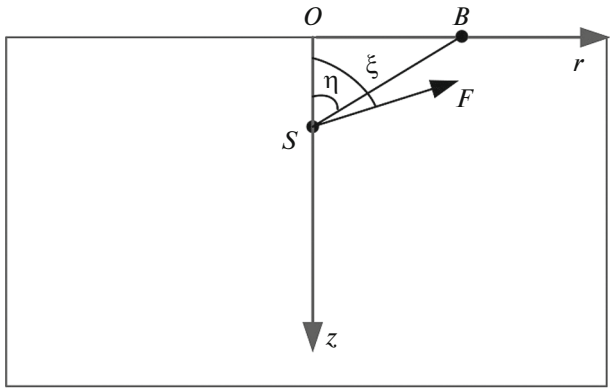

Fig. 10. Schematic of the azimuth angle of observation point.

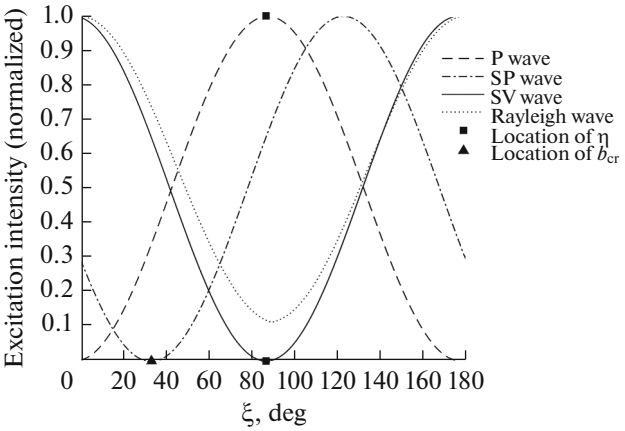

Fig. 11. The relationship of intensity of each wave to the direction of force.

the intensity of the Rayleigh wave is closely related to the ratio of the source depth to wavelength of the Rayleigh wave. Through numerical simulation, the relationship between them is plotted in Fig. 9.

As shown in Fig. 9, intensity of the Rayleigh wave is maximum on the surface and decays rapidly with the source depth increases. It can be found that most of energy of the Rayleigh wave is within a wavelength range below the surface.

II. The Single Force with Different Direction

Here, the relationships of intensity of each wave on the surface to the direction of single force are studied. It is convienent to introduce the angle η to represent the azimuth angle of observation point (Fig. 10).

Only the acoustical field in the plane $\theta = 0$ is considered. The single force source is set at a depth of 30 mm with the direction angle ξ. The intensity of each wave is obviously related to the direction angle ξ of the single force. Figure 11 displays the relationship of intensity of the P wave, SP wave, SV wave, and Rayleigh wave on the surface to the direction angle ξ, respectively. The intensity of each wave is represented by the total particle displacement and normalized by its maximum.

The azimuth angle η of point *B* can be calculated to be about 86.5° with the medium paremeters in this paper. And the location of η and b_{cr} are also given in Fig. 11.

Some interesting conclusions can be obtained from Fig. 11, namely:

(1) When $\xi = \eta$, the SV wave cannot be observed at the observation point, but the intensity of P wave reaches its maximum. Besides, when $\xi = \eta + \pi/2$, the

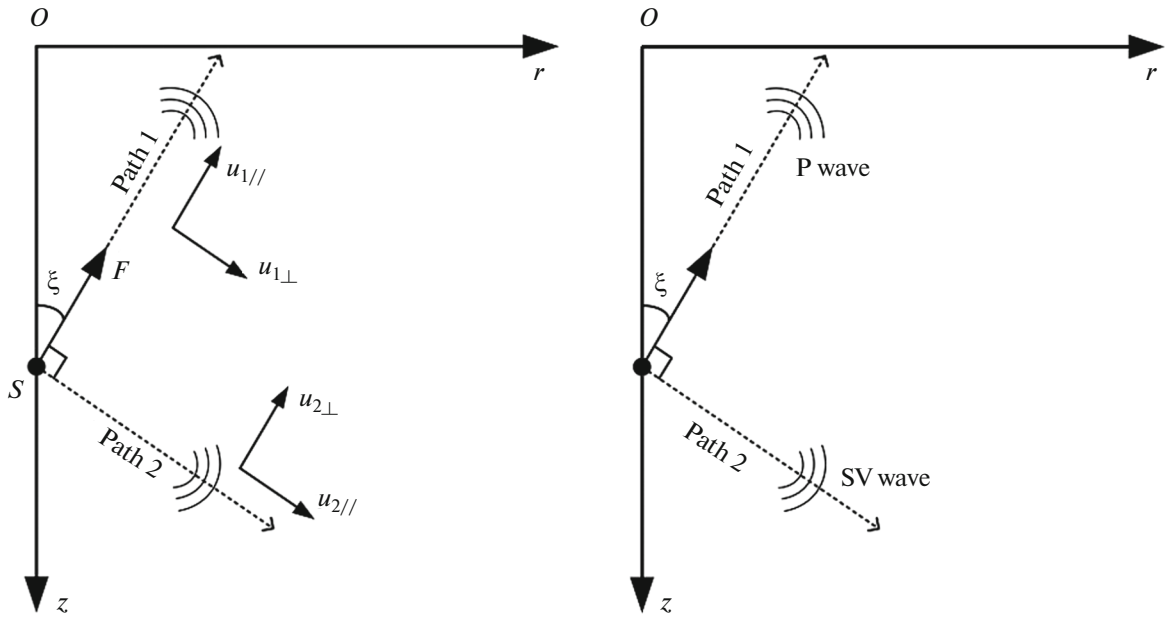

Fig. 12. Sketch of wave propagating on two special paths.

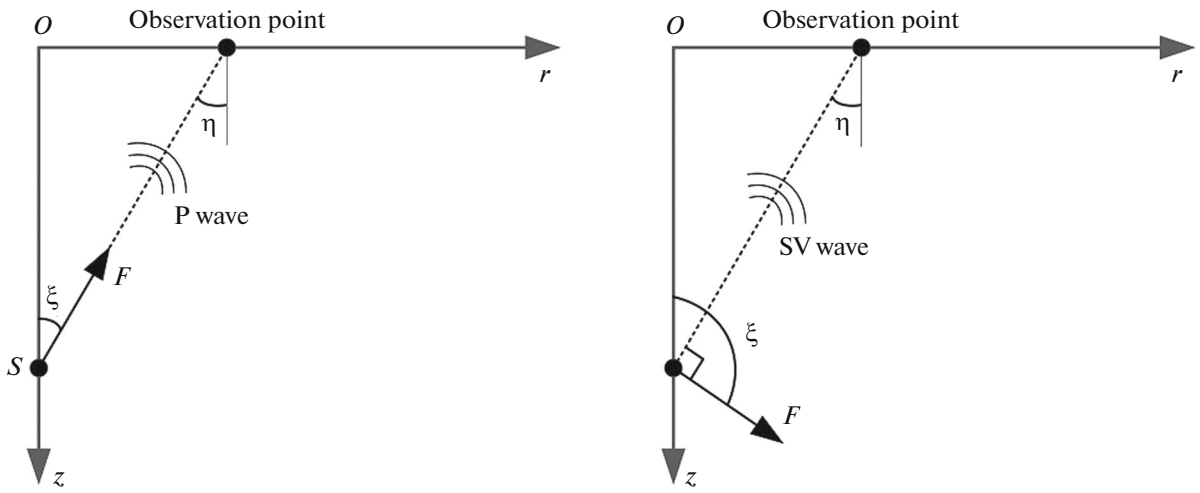

Fig. 13. Sketch of wave propagating in two special cases: (a) $\xi = \eta$, (b) $\xi = \eta + \pi/2$.

P wave cannot be observed at the observation point, but the intensity of SV wave reaches its maximum.

In Fig. 12, the dotted line are two propagation paths of wave. The path 1 is in the direction of the single force, and the path 2 is perpendicular to the direction of the single force. In Fig. 12a, according to formulas (7), (16) and (18), it can be proved that the particle displacements on two propagation paths satisfy

$$u_{1\parallel} \neq 0,\ u_{1\perp} = 0,\ \ u_{2\parallel} = 0,\ u_{2\perp} \neq 0. \qquad (23)$$

Formula (23) shows that only the P wave can propagate on path 1, and only the SV wave can propagate on path 2, as shown in Fig. 12b.

It can be concluded that on the propagation path in the direction of the single force, only P wave can propagate. Similarly, on the propagation path perpendicular to the direction of the single force, only SV wave can propagate.

So, as shown in Fig. 13a, when $\xi = \eta$, only the P wave can be observed at the observation point. In Fig. 13b, when $\xi = \eta + \pi/2$, only the SV wave can be observed at the observation point.

(2) The most peculiar case is, when $\xi = b_{cr}$, the SP wave cannot be observed anywhere on the boundary. Because only the SP wave reflected by SV wave incident at the incident angle b_{cr} can propagate along the

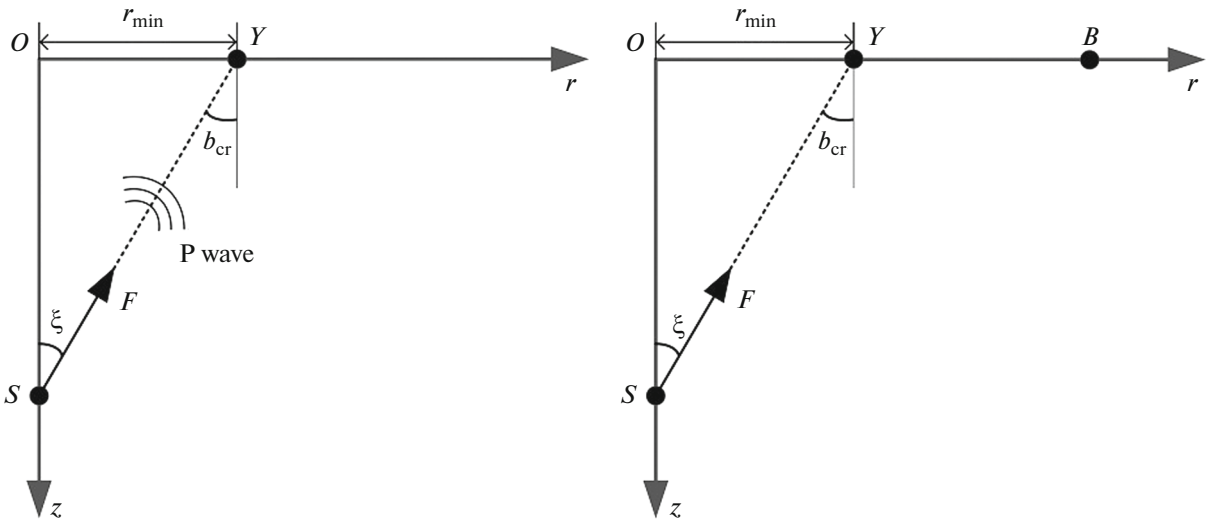

Fig. 14. Sketch of SP wave not being formed.

boundary. But as shown in Fig. 14a, when $\xi = b_{cr}$, there is no SV wave propagating on the propagation path in the direction of the single force. So, in this case, the SP wave cannot be formed. (The point Y is the critical point where the SP wave can be formed, not the observation point).

As shown in Fig. 14b, the single force source is set at a depth of 15 mm with the direction angle $\xi = b_{cr}$. And the observation point B is set at a horizontal distance of 500 mm from the origin. Then the particle displacements at point B are given in Fig. 15.

In Fig. 15, the SP wave cannot be observed on the boundary, compared with the displacement waveforms in Fig. 8.

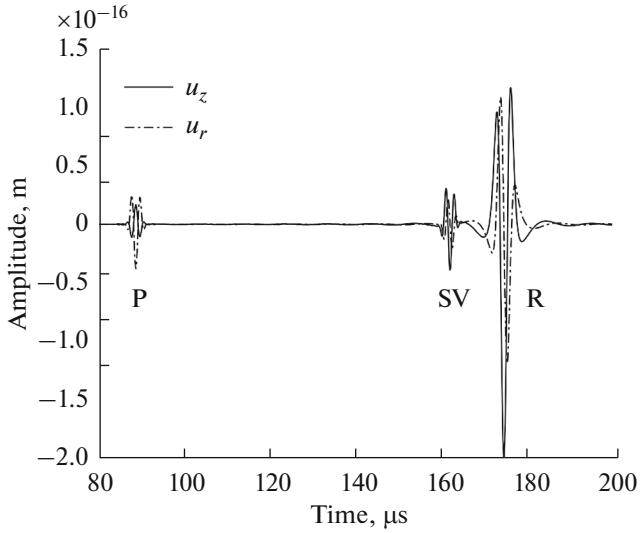

Fig. 15. The particle displacement waveforms at point B with $\xi = b_{cr}$.

(3) The intensity curve of the Rayleigh wave is very similar to that of SV wave, it shows that the energy of the Rayleigh wave may originate mainly from the SV wave. But the minimum intensity of the Rayleigh wave is not zero, which shows that the energy of the Rayleigh wave originates from the inhomogeneous SP wave, not the SP wave being observed on the boundary or the reflected SV wave.

3. CONCLUSIONS

With the advantage of B, P, C coordinate system, the mathematical expressions of acoustic field excited by the single force with arbitrary direction in semi-infinite elastic space are obtained in this paper. It is shown by the mathematical expressions that the P wave or SV wave cannot satisfy the free boundary conditions in the semi-infinite elastic space independently. In order to satisfy the free boundary conditions, the P wave or SV wave generates not only reflected wave but also converted wave when they reach the boundary. It is found by numerical simulation that there are several kinds of waves in the semi-infinite elastic space: direct P wave, direct SV wave, SP wave propagating along the free surface which can generate Head wave and Rayleigh wave. Then, the relationships of the direction of single force to the excitation intensity of each wave on the free surface are deeply studied. It is found that on the propagation path in the direction of the single force, only P wave can propagate. And on the propagation path perpendicular to the direction of the single force, only SV wave can propagate. It is also found that the SP wave cannot be observed anywhere on the boundary when the direction of single force (ξ) is equal to the critical reflection angle (b_{cr}). Interestingly, it can be speculated that the energy of the Rayleigh wave may origi-

nate mainly from the SV wave, more precisely the inhomogeneous SP wave converted by the SV wave. Besides, the relationship of the Rayleigh wave intensity to ratio of source depth to wavelength is obtained. The Rayleigh wave decays rapidly as the source depth increases.

ACKNOWLEDGMENTS

The study was supported by the National Natural Science Foundation of China (nos. 11774377, 11574343, 11474308).

REFERENCES

1. F. R. Breckenridge, C. E. Tschiegg, and M. Greenspan, J. Acoust. Soc. Am. **57** (3), 626 (1975).
2. A. Mourad and M. Deschamps, J. Acoust. Soc. Am. **97** (5), 3194 (1995).
3. M. Spies, J. Acoust. Soc. Am. **102** (4), 2438 (1997).
4. A. Moura, J. Acoust. Soc. Am. **127** (3), 1185 (2010).
5. S. V. Kuznetsov and E. O. Terentjeva, Acoust. Phys. **61** (3), 356 (2015).
6. A. E. Love, Proc. London Math. Soc. **1**, 291 (1904).
7. T. Matuzawa, J. Astron. Geophys. **4**, 1 (1926).
8. R. Sato, J. Phys. Earth **17**, 101 (1969).
9. I. Onda, S. Komaki, and M. Ichikawa, J. Phys. Earth **23**, 205 (1975).
10. Yu. V. Petukhov, A. V. Razin, and V. A. Razin, Acoust. Phys. **55**(3), 425 (2009).
11. W. M. Ewing, W. S. Jardetsky, and F. Press, Phys. Today **10** (12), 27 (1957). W. M. Ewing, W. S. Jardetsky, and F. Press, *Elastic Waves in Layered Media* (McGraw-Hill, New York, 1957).
12. M. Yu. Dvoesherstov, V. A. Savin, and V. I. Cherednik, Acoust. Phys. **47** (6), 682 (2001).
13. M. A. Kulesh, E. F. Grekova, and I. N. Shardakov, Acoust. Phys. **55** (2), 218 (2009).
14. M. G. Markov, I. A. Markova, and S. N. Sadovnichiy, Acoust. Phys. **56** (3), 299 (2010).
15. V. F. Dmitriev and A. N. Noskov, Acoust. Phys. **56** (4), 475 (2010).
16. A. D. Lapin, Acoust. Phys. **50** (2), 192 (2004).
17. A. I. Korobov, Yu. A. Brazhkin, and E. S. Sovetskaya, Acoust. Phys. **56** (4), 446 (2010).
18. V. A. Gusev and O. V. Rudenko, Acoust. Phys. **56** (6), 861 (2010).
19. C. Han-yin, J. Trevelyan, and S. Johnstone, J. Acoust. Soc. Am. **130** (1), EL44 (2011).
20. C. Han-yin, Z. Bi-Xing, S. Johnstone, and J. Trevelyan, J. Acoust. Soc. Am. **131** (3), 2048 (2012).
21. A. Ben-Menahem and S. J. Singh, Bull. Seismol. Soc. Am. **58**, 1519 (1968).
22. Y. Zhen-Xing, Acta Geophys. Sin. **22**, 181 (1979).
23. Z. Bi-Xing, M. Yu, C. Q. Lan, and W. Xiong, J. Acoust. Soc. Am. **100** (6), 3527 (1996).
24. N. L. Batanova, A. V. Golenishchev-Kutuzov, V. A. Golenishchev-Kutuzov, and R. I. Kalimullin, Acoust. Phys. **50** (5), 496 (2004).
25. Yu. M. Zaslavskii, B. V. Kerzhakov, and V. V. Kulinich, Acoust. Phys. **51** (5), 554 (2005).
26. Yu. M. Zaslavskii and V. Yu. Zaslavskii, Acoust. Phys. **55** (6), 910 (2009).
27. L. S. Zagorskii and V. L. Shkuratnik, Acoust. Phys. **59** (2), 197 (2013).